# Project Phase 2 Report

# Reliability Assessment for Utility PV Inverter System

Project period: Dec 2022 – Dec 2023

Project team: Qiang Mu (Ph.D. student), Jiale Zhou (Ph.D. student), Dr. Tiefu Zhao (PI)

UNC Charlotte

Tiefu.Zhao@Charlotte.edu

## Project Scope

The reliability of power electronics is critical for energy conversion systems to maintain safety, efficiency, and uptime. PV inverters are regarded as one of the most fragile components in PV systems. Their failures can downgrade the system efficiency, cause catastrophic system breakdowns, and result in expensive economic losses. U.S. Department of Energy (DOE) Solar Energy Technologies Office (SETO) considered "improving reliability and efficiency of new and existing PV technology" as the key focus for increasing PV useful system life to 50 years while lowering the cost of energy. Based on DOE's recent PV system failure survey [1], occurrences of specific hardware issues are shown as percentage and in Fig. 1. PV inverters are associated with 40% or more of the service requests, representing the single largest category in the PV system failure causes.

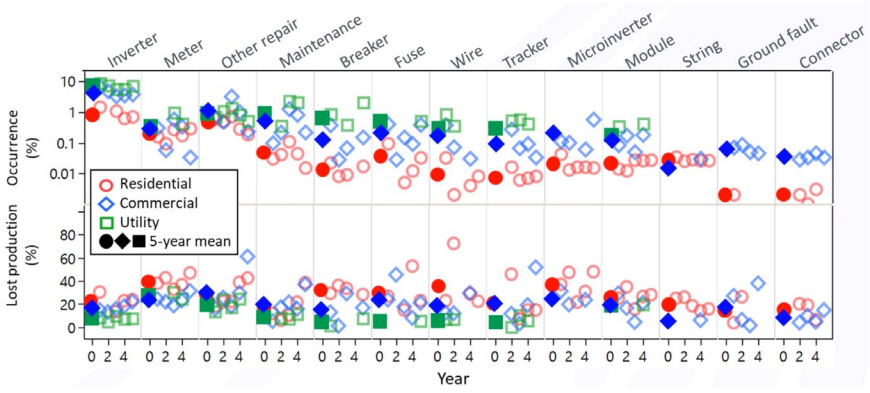


Fig. 1 PV system hardware failures (data based from100k+ systems in the U.S.) [1]

Among all the various failure causes investigated by researchers, thermal stress has been identified as one of the significant causes of PV inverter modules. The generated power due to the chaining irradiation usually has a large variation in a short duration. The solar inverters will bear such variation of the real power from hundreds of kilowatts to several megawatts. Subsequently, a fast-varying power loss is accompanied and aggregated, and a severe thermal cycling occurs in the power module of the converter. Both the bond-wire liftoff and the solder joint fatigue, two

most frequent failure modes of power modules, have been justified related to this thermal stress. This thermal stress accelerates the degradation of semiconductor devices, downgrades the system quality and efficiency, and eventually causes catastrophic system breakdowns and extensive economic losses. Therefore, it is critical to establish a **reliability assessment tool** to quantitively assess PV inviter's reliability based on the field data and support the development of safer and more reliable PV.

## Project Achievements

The phase 1 project team has been focused on developing a reliability assessment tool to quantitively assess PV inverter's reliability based on Duke energy's field data at the Mount Holly PV system. Fig. 2 shows the overall framework of the proposed reliability assessment tool for PV inverter. The proposed approach introduces the PV system reliability-related information (such as energy mission profile, semiconductor temperature and stress, temperature, solar irradiation, etc.) into the inverter control system, therefore offers a universal platform to quantify and compare the reliabilities for PV inverter from different vendors with different control methods.

The phase 2 project team has been focused on developing a statistical approach based on the Monte Carlo analysis, as shown in Fig. 14. By doing so, variations in model parameters and thermal stresses can be introduced to represent uncertainties. Then, the distribution of power device lifetime can be obtained. This approach helps PV inverter designers select the most cost-effective power device and justify the corresponding risk of unreliability among the options available in the market for a specific PV inverter application. Additionally, system-level reliability assessment can be performed using reliability block diagrams. The obtained lifetime results can be used in a comparative manner to evaluate the impact of the PV inverter topology on the expected lifetime of the PV inverter system.

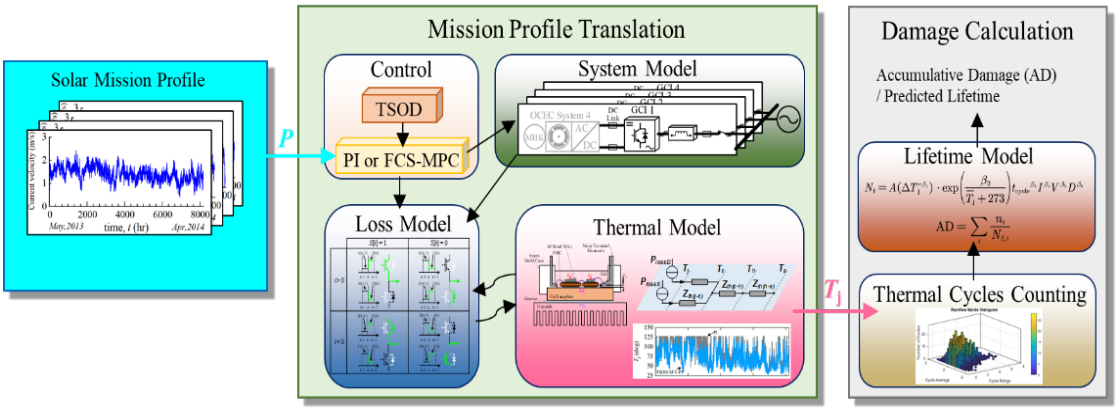


Fig. 2 Reliability assessment framework for utility PV system

The reliability assessment framework was based on the real field data from Duke energy's Mount Holly PV system. Examples of the yearly three-phase current data are illustrated in Fig. 3. The data has been processed to generate the mission profile as the input to the reliability assessment

framework. The output of the framework is the accumulative damage (AD) and predicted lifetime of the semiconductors. The quantified accumulative damage is highly related to the semiconductor specs, PV inverter topology, package and cooling system, and ambient temperature variation. The results in Fig. 4 are representative and will be refined once we have the detailed design and specifications from the inverter vendor. The framework provides a universal tool to quantitatively compare the reliabilities for PV inverters from different vendors with different control methods. The lifetime prediction for the PV inverter leads to a better understanding of the thermal stress impact to inverter failure. Based on this reliability assessment platform, predictive maintenance and reliability-oriented control and operation methods, such as active thermal control, can be evaluated to extend the lifetime of PV inverters.

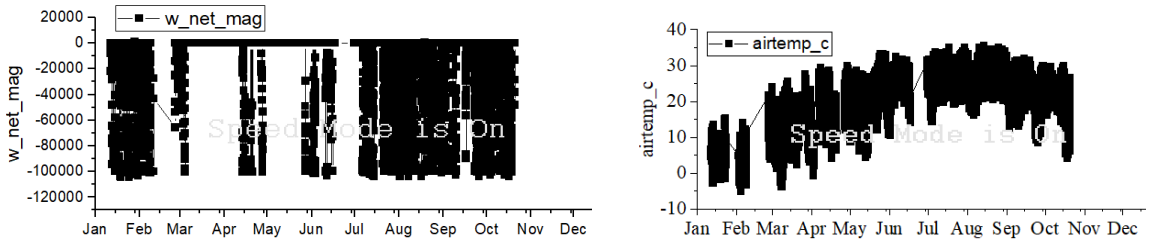


(a) w_net_mag: Active power (b) airtemp_c: ambient temperature

Fig. 3 Yearly mission profiles from Mount Holly PV system

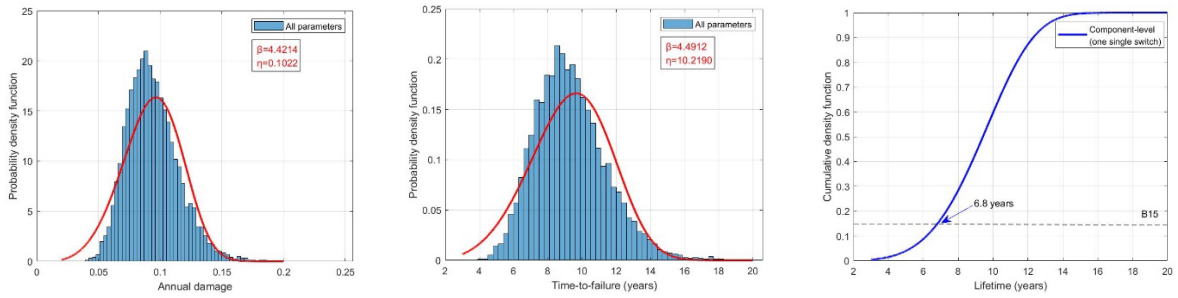


(a) (b) (c)

Fig. 4. Monte Carlo analysis considering all parameters variations from the stress evaluation and lifetime model. (a) Annual damage; (b) Time-to-failure distribution; (c) Cumulative density function (i.e. unreliability) along with the lifetime (IGBT).

As future work, the team plans to evaluate the PV inverter reliabilities for different control and operation strategies and provide lifetime extension recommendations based on the Phase 2 case study of the Mount Holly PV system. The team will also investigate arc safety and fire resilience for PV and utility energy storage systems to support the development of safe and reliable utility PV and energy storage systems.

More details about the reliability assessment are given in the **Appendix (technology descriptions**).

## Acknowledgments

The team would like to thank Dr. Kevin Chen, Tom Fenimore, and Dwayne Bradley from Duke Energy for their valuable guidance and technical discussions and for providing field data to this project.

# Appendix: Technology Descriptions

## I. Technology Description

The lifetime of power converters in PV systems suffers from intermittent renewable energy generation which is highly affected by instantaneous environmental conditions. The generated power or the mission profile usually has a large variation in a short duration [2]. Because of the inline structure, power converters will bear such variation of the real power from hundreds of kilowatts to several megawatts. This variation not only induces the surge and the slump of the power flow on the converter, which increases control requirements in both transient and steady states, but also arises a fast-varying power loss across the power converter. This varying power loss is rapidly aggregated inside of the power module in the form of heat which produces a severe thermal cycling in the power converter over the mission profile. Fig. 5 shows the overall framework of the proposed reliability assessment tool for PV inverter. Fig. 6 demonstrates the lifetime prediction procedure of semiconductor modules.

There are mainly four steps in the lifetime prediction process of the power semiconductor devices in the PV inverter applications. In the first step, loss model will be established from the input data, such as device characteristics, converter features. Then, in the second step, a junction temperature look-up table will be established with the thermal characteristics of the power semiconductor devices and the mission profiles of PV inverter applications. In step 3, the different thermal stress factors, such as junction temperature swing ($\Delta T_j$) and mean junction temperature ($\overline{T_j}$), are obtained from the junction temperature profiles by using Rainflow counting algorithm. Finally, the lifetime of the power semiconductor devices is obtained based on linear damage accumulation rule.

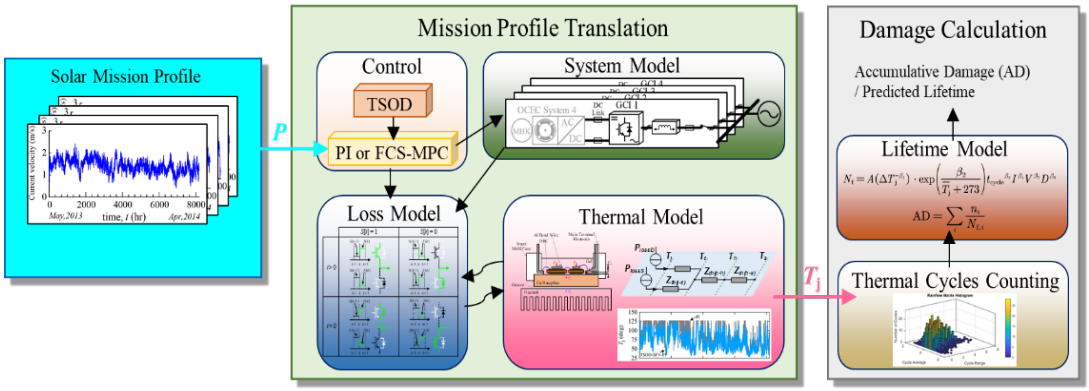


Fig. 5 Reliability assessment framework for utility PV system

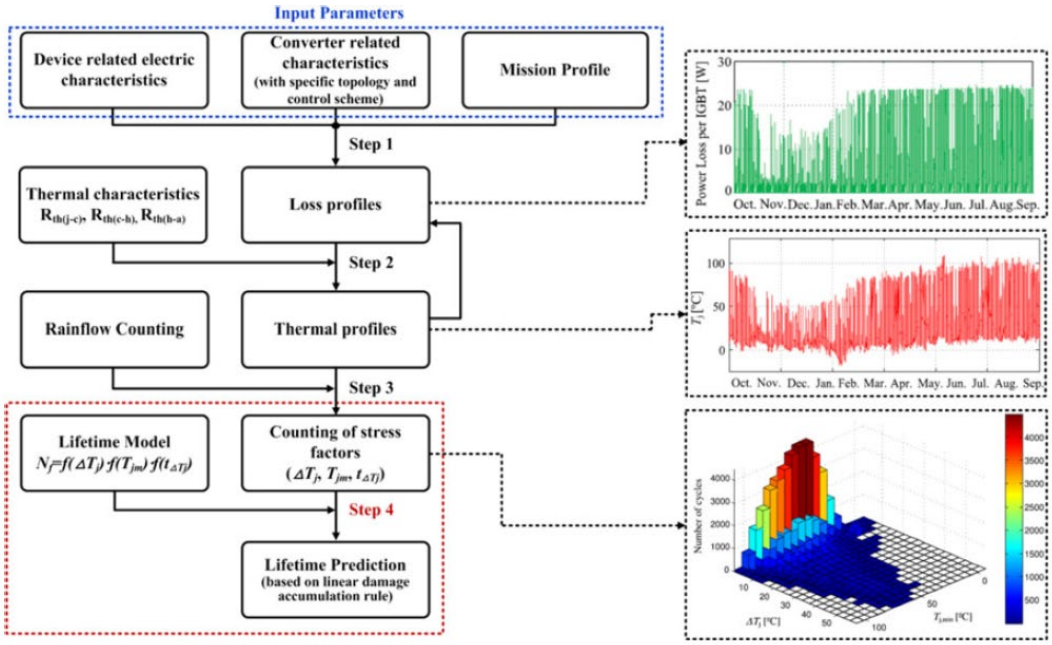


Fig. 6 Lifetime prediction procedure of IGBT modules in PV inverter applications [3].

## *A. Loss Model*

An energy-based loss model of the power module has been established in the project. The power loss in power modules consists of two parts, the conduction loss and the switching loss, coming from the active switch (IGBT, MOSFET, etc.,) and the antiparallel diode, respectively. The conduction state and switching events for the half-bridge semiconductor devices against the current and the switching state are shown in Fig. 7, where it covers both upper and lower level switches. All dynamic actions are summarized for the hard switching on the half bridge.

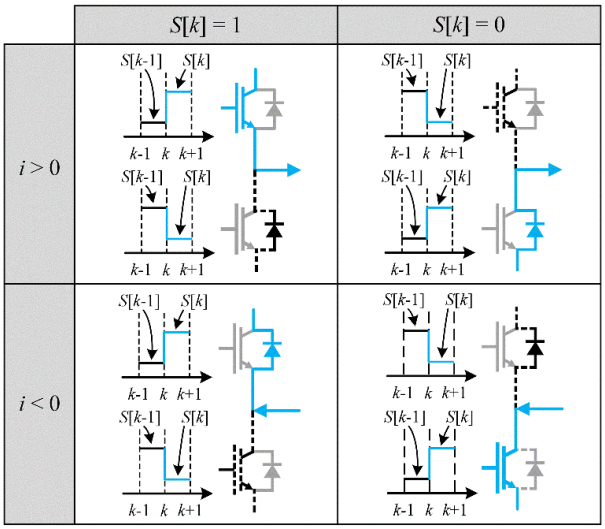


Fig. 7 Conduction states and switching events of the grid-tied inverter.

Switching loss in terms of the pulse energy happens when the semiconductor device turns on or off for the current commutation. This switching loss can be calculated by using the curve fitting and the behavioral loss model [4].

$$E_{switch} = \begin{cases} E_{on}(\boldsymbol{i}_{abc}, T_j) \cdot V_{CE} / V_{CE,rated}, & \triangle \boldsymbol{s}_{abc} = 1 \\ 0, & \triangle \boldsymbol{s}_{abc} = 0 \\ E_{off}(\boldsymbol{i}_{abc}, T_j) \cdot V_{CE} / V_{CE,rated}, & \triangle \boldsymbol{s}_{abc} = -1 \end{cases} \tag{1}$$

where the switching loss depends on the line current $\boldsymbol{i}_{abc}$ for each phase, the blocking voltage $V_{CE}$ that is $V_{DC}$ in the two-level converter, the junction temperature $T_j$ and the successive switching states.

Conduction loss is the power dissipated on the semiconductor device during the device on-state. The conduction loss can be estimated in terms of the uniform energy [4].

$$E_{cond} = \begin{cases} T_s \cdot P_{cond} = T_s \cdot v_{CE,ON}(\boldsymbol{i}_{abc}, T_j) \cdot \boldsymbol{i}_{abc}, & \boldsymbol{s}_{abc}[k+1] = 1 \\ 0, & \boldsymbol{s}_{abc}[k+1] = 0 \end{cases} \tag{2}$$

where $v_{CE,ON}$ is the voltage drop on the semiconductor device during the on-state which is determined by curve fitting with the current $\boldsymbol{i}_{abc}$ and the junction temperature $T_j$.

Then, the total energy-based power loss for all bridges can be calculated in the sum of the switching loss and conduction loss.

$$\boldsymbol{E}_{abc}[k] = \sum_{a,b,c} (E_{switch}[k] + E_{cond}[k]) \tag{3}$$

It is noted that both switching loss and conduction loss vary with the junction temperature. The amount of power loss would change significantly over a broad range of the junction temperature, even if the converter is operating under the same power loading. Furthermore, the power loss would have feedback on the junction temperature, which complicates the system dynamic analysis. Therefore, the junction temperature of the power model has to be identified in the proposed control method.

*B. Thermal Model*

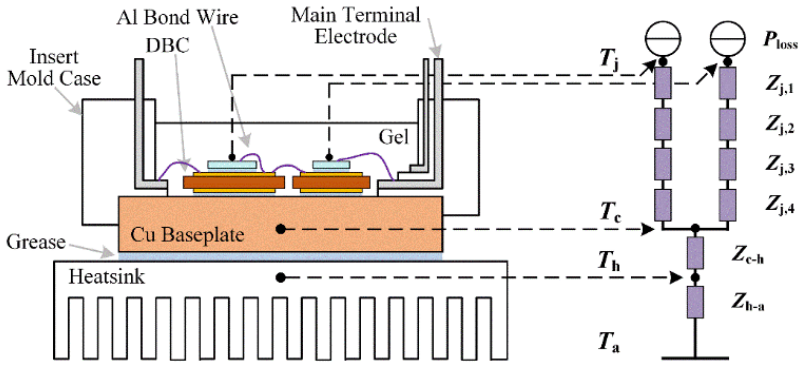


Fig. 8 Structure of the power module and its Foster-type RC thermal model

The junction temperature of the power module is retrieved through the real-time estimation in the most scenarios. The common way to estimate it is through a thermal resistance and capacitance (RC) model and a simple case or heatsink temperature feedback [5]. Fig. 8 shows a Foster-type RC model of power modules, including four layers of the junction-to-case thermal impedance, one layer of the case-to-heatsink thermal impedance and one layer of the heatsink-to-air thermal impedance. Each thermal impedance consists of one lumped RC which only infers the mathematical fitting of the temperature curve and has no physical meanings.

The parameters of the Foster-type RC thermal model are provided based on the transient thermal impedance curve in the datasheet provided by the manufacturer. Thermal resistance and thermal capacitance are used to obtain the frequency domain representation of the thermal impedance. And the junction temperature of the power module \is estimated as

$$T_j = P_{loss} \sum_{i=1}^{n} Z_{j,i} + T_c = P_{loss} \sum_{i=1}^{n} \frac{R_i}{\tau_i s + 1} + T_c \tag{4}$$

where $P_{loss}$ is the output from the loss model, $R_i$ and $\tau_i$ are the thermal resistance and time constant for the layer $i$ of thermal model, $T_c$ is the case temperature feedback which can be measured through a low-bandwidth thermocouple or a linear thermal sensor.

*C. Lifetime Prediction*

The reliability assessment is conducted by accumulative damage and lifetime prediction. In this project, the Bayerer's IGBT lifetime model and Miner's rule are used to calculate the

accumulative damage (AD) and the predicted lifetime based on the thermal cycles counting results [6].

$$N_{\mathrm{f}} = A(\Delta T_{\mathrm{j}}^{-\beta_1}) \cdot \exp\left(\frac{\beta_2}{\overline{T}_{\mathrm{j}} + 273}\right) t_{\mathrm{cycle}}{}^{\beta_3} I^{\beta_4} V^{\beta_5} D^{\beta_6} \tag{5}$$

$$\mathrm{AD} = \sum_i \frac{n_i}{N_{\mathrm{f},i}} \tag{6}$$

where $N_{\mathrm{f}}$ is defined as the number of cycles to failure for the specific thermal stress ($\overline{T}_{\mathrm{j}}$, $\Delta T_{\mathrm{j}}$, $t_{\mathrm{cycle}}$), $n_{\mathrm{i}}$ is the number of this thermal stress, $I$ is the current per wire bond, $V$ is the voltage class, and $D$ is the diameter of the bond wire. Parameters $A$ and $\beta_{1\text{-}6}$ are device dependent constants according to the aging data provided by manufacturers [6]. The lifetime prediction is calculated by reciprocal of AD. When AD equals to one, the device is regarded to be fully failure out.

## II. Reliability Accessment

The first step of the reliability assessment is to determine the mission profiles of PV inverters. Fig. 9 shows the yearly PV system current, voltage, and weather data from Mount Holly PV system. Fig. 10 represents the active power and ambient temperature mission profiles. The power rand temperature data are utilized to the reliability assessment project. Due to some missing data in ambient temperature mission profiles, assumptions have been made in the ambient temperature mission profile to fill up some of the missing temperatures. For example, there is no data recording of the ambient temperature from Feb. 9 to Feb. 24, the adjacent weeks' ambient temperatures are added in these blank positions.

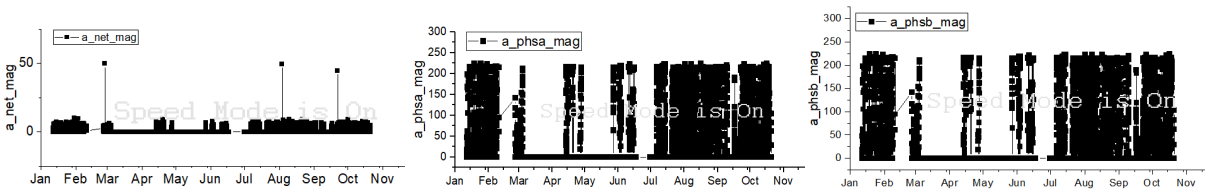


(a) a_net_mag: three-phase current (b) a_phsa_mag: Phase A current (c) a_phsb_mag: Phase B current

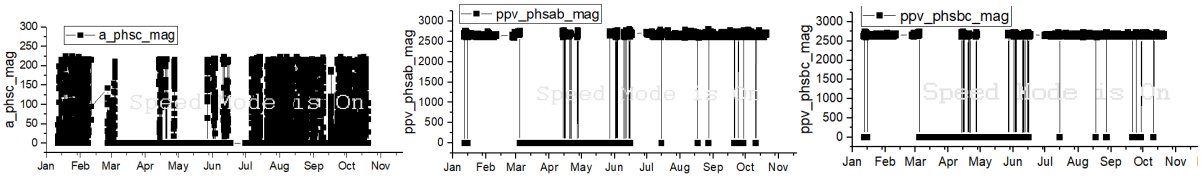


(d) a_phsc_mag: Phase C current (e) ppv_phsab_mag: Vab (f) ppv_phsbc_mag: Vbc

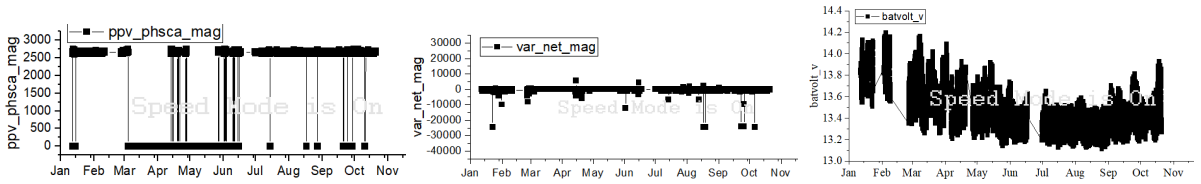


(g) ppv_phsca_mag: Vca (h) var_net_mag: Reactive power (i) batvolt_v: Battery voltage

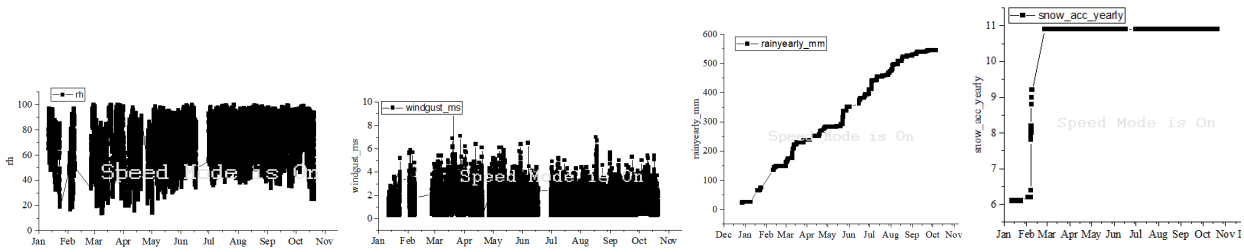


(j) rh (k) windgust (l) rain (m) snow

Fig. 9 Yearly mission profiles from Mount Holly PV system

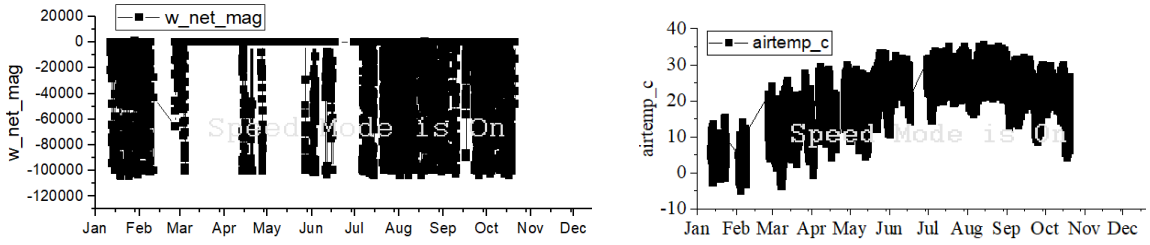


(a) w_net_mag: Active power (b) airtemp_c: ambient temperature

Fig. 10 Active power and ambient temperature mission profiles

Simulations are developed in MATLAB/Simulink and PLECS environment according to the PV grid-tied inverter topologies shown in Fig. 11. The active power shown in Fig. 10 (a) is no more than 110kW, and the range of ambient temperature shown in Fig. 10(b) is from -10℃ to 40℃. Therefore, the simulation parameters are selected from Table I. The thermal model of Infineon FF300R12RT4 IGBT module including IGBT device and anti-parallel diode is applied in the simulation procedure. The mean junction temperature look-up tables of IGBT device and

anti-parallel diode are obtained by simulating with different power loadings and ambient temperature. As illustrated in Table II and III, the simulation results cover all the operating conditions of PV inverter in this project.

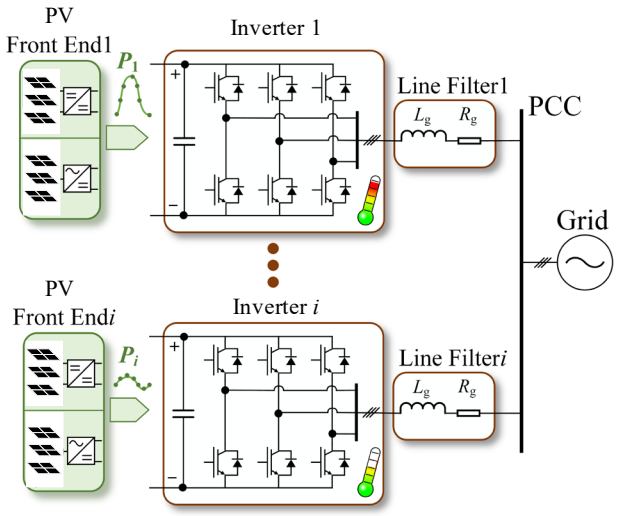


Fig. 11 PV grid-tied inverter topologies.

TABLE I SIMULATION PARAMETERS

| | |
|---|---|
| Rated power $P$ | 110kW |
| Rated DC bus voltage $V_{dc}$ | 800V |
| Grid frequency $f$ | 60Hz |
| Rated AC grid voltage $\boldsymbol{e}_{abc}$ ($V_{LN}$/$V_{LL}$) | 160/277V |
| Line current $\boldsymbol{i}_{abc}$ (RMS) | 230A |
| Line inductance $L_g$ | 3mH |
| DC bus capacitance $C$ | 940μF |
| IGBT module | Infineon FF300R12RT4 |

TABLE II JUNCTION TEMPERATURE OF IGBT LOOK-UP TABLE

| $T_a$ / $P_{load}$ | -10℃ | -5℃ | 0℃ | 5℃ | 10℃ | 15℃ | 20℃ | 25℃ | 30℃ | 35℃ | 40℃ |
|---|---|---|---|---|---|---|---|---|---|---|---|
| 0kW | -10 | -5 | 0 | 5 | 10 | 15 | 20 | 25 | 30 | 35 | 40 |
| 10kW | -3.5 | 1.6 | 6.8 | 11.9 | 17.0 | 22.2 | 27.3 | 32.4 | 37.6 | 42.7 | 47.9 |
| 20kW | 2.5 | 7.8 | 13.0 | 18.3 | 23.5 | 28.8 | 34.0 | 39.3 | 44.5 | 49.8 | 55.0 |
| 30kW | 8.2 | 13.5 | 18.9 | 24.2 | 29.6 | 34.9 | 40.1 | 45.6 | 51.0 | 56.4 | 61.8 |
| 40kW | 14.0 | 19.4 | 24.9 | 30.6 | 35.8 | 41.2 | 46.7 | 52.2 | 57.7 | 63.2 | 68.8 |
| 50kW | 20.3 | 25.9 | 31.5 | 37.0 | 42.6 | 48.1 | 53.8 | 59.4 | 65.0 | 70.7 | 76.4 |
| 60kW | 26.8 | 32.5 | 38.2 | 43.8 | 49.5 | 55.3 | 61.1 | 66.8 | 72.6 | 78.5 | 84.4 |
| 70kW | 33.9 | 39.7 | 45.5 | 51.4 | 57.3 | 63.2 | 69.2 | 75.1 | 81.2 | 87.2 | 93.3 |

| | | | | | | | | | | | |
|---|---|---|---|---|---|---|---|---|---|---|---|
| 80kW | 41.4 | 47.3 | 53.3 | 59.4 | 65.4 | 71.5 | 77.7 | 83.9 | 90.2 | 96.5 | 102.9 |
| 90kW | 49.3 | 55.5 | 61.7 | 67.9 | 74.3 | 80.7 | 87.1 | 93.6 | 101.1 | 106.9 | 113.6 |
| 100kW | 51.1 | 57.2 | 63.2 | 69.5 | 75.8 | 82.2 | 88.5 | 95.0 | 101.5 | 108.4 | 114.9 |
| 110kW | 52.7 | 58.9 | 65.1 | 71.3 | 77.6 | 84.0 | 90.3 | 96.7 | 103.3 | 109.9 | 116.5 |

TABLE III JUNCTION TEMPERATURE OF DIODE LOOK-UP TABLE

| $T_a$ / $P_{load}$ | -10℃ | -5℃ | 0℃ | 5℃ | 10℃ | 15℃ | 20℃ | 25℃ | 30℃ | 35℃ | 40℃ |
|---|---|---|---|---|---|---|---|---|---|---|---|
| 0kW | -10 | -5 | 0 | 5 | 10 | 15 | 20 | 25 | 30 | 35 | 40 |
| 10kW | -4.1 | 1.0 | 6.3 | 11.5 | 16.7 | 21.8 | 27.0 | 32.2 | 37.4 | 42.6 | 47.8 |
| 20kW | 1.4 | 6.8 | 12.2 | 17.5 | 22.9 | 28.3 | 33.7 | 39.0 | 44.4 | 49.8 | 55.2 |
| 30kW | 6.5 | 12.0 | 17.5 | 23.3 | 28.5 | 34.1 | 39.6 | 45.1 | 50.6 | 56.1 | 61.7 |
| 40kW | 11.5 | 17.2 | 22.8 | 28.5 | 34.1 | 39.8 | 45.5 | 51.1 | 56.8 | 62.4 | 61.2 |
| 50kW | 16.9 | 22.7 | 28.5 | 34.3 | 40.5 | 45.8 | 51.6 | 57.4 | 63.3 | 69.1 | 74.9 |
| 60kW | 22.3 | 28.2 | 34.1 | 40.0 | 45.9 | 51.9 | 57.8 | 63.8 | 69.7 | 75.7 | 81.7 |
| 70kW | 28.1 | 34.1 | 40.2 | 46.2 | 52.3 | 58.4 | 64.5 | 70.6 | 76.7 | 82.9 | 89.0 |
| 80kW | 34.0 | 40.1 | 46.4 | 52.6 | 58.8 | 65.0 | 71.3 | 77.6 | 83.9 | 90.2 | 96.6 |
| 90kW | 40.2 | 46.6 | 52.9 | 59.3 | 65.7 | 72.2 | 78.6 | 85.1 | 91.6 | 98.1 | 104.7 |
| 100kW | 39.9 | 46.2 | 52.3 | 58.6 | 64.9 | 71.2 | 77.7 | 83.9 | 90.2 | 96.7 | 103.2 |
| 110kW | 39.9 | 46.1 | 52.2 | 58.2 | 64.5 | 70.5 | 76.9 | 83.0 | 89.3 | 95.7 | 102.0 |

After the simulation, junction temperature swing $\Delta T_j$ and mean junction temperature $T_{jmean}$ are obtained by using Rainflow counting method, and the results are illustrated in Fig. 12. The mean junction temperature mission profiles of IGBT and anti-parallel diode is from January of 2021 to October of 2021. The rainflow matrix histogram shows the cycle counts of corresponding thermal stress (The mean junction temperature and the junction temperature swing).

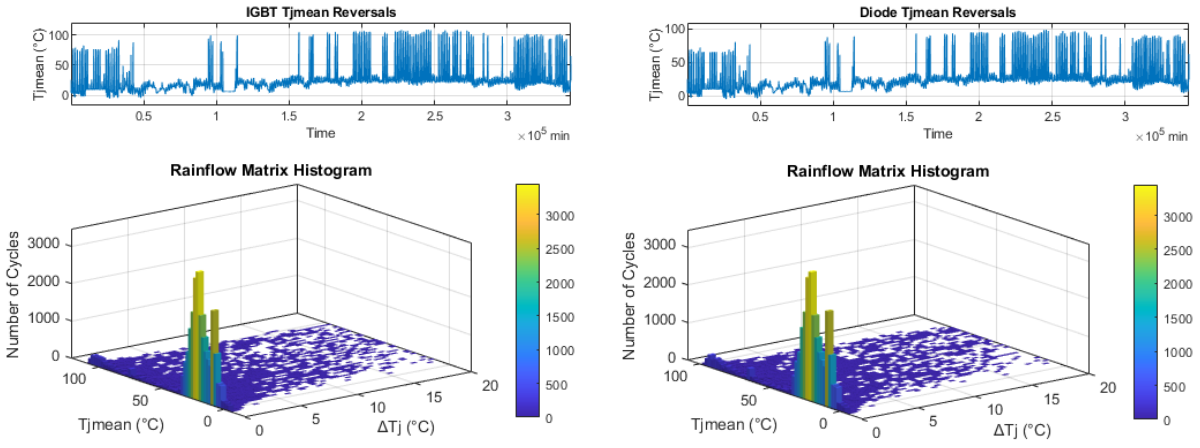


Fig. 12 Rainflow counting results and the mean junction temperature profiles.

TABLE IV SIMULATION PARAMETERS

| | |
|---|---|
| $\beta_1$ | -4.416 |
| $\beta_2$ | 1285 |
| $\beta_3$ | -0.463 |
| $\beta_4$ | -0.716 |
| $\beta_5$ | -0.761 |
| $\beta_6$ | -0.19 |
| ~~$t_{cycle}$~~ | ~~400~~ |
| V | 1200 |
| D | $150*10^{-5}$ |
| A | $9.34*10^{14}$ |
| I | 300 |

In the final step, lifetime prediction is conducted by equations (5) and (6) in the MATLAB/Simulink environment. The simulation parameters are presented in Table IV [6].

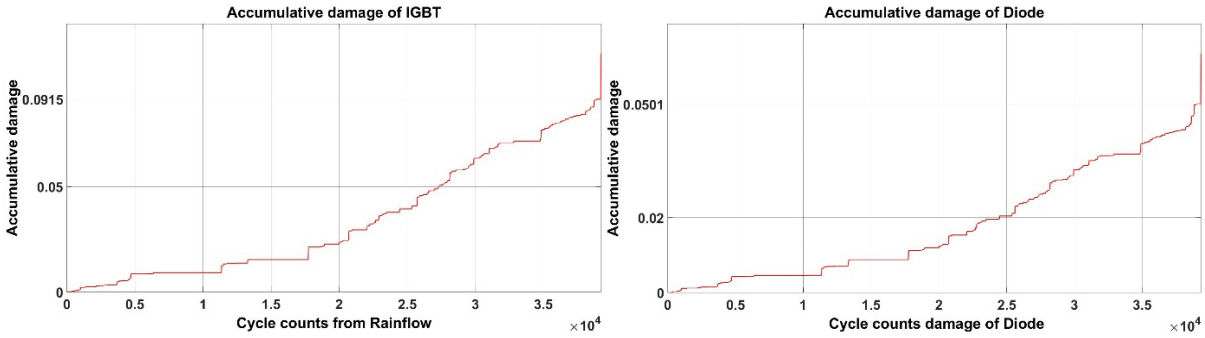


(a) Accumulative damage of IGBT (b) Accumulative damage of Diode

Fig. 13 Accumulative damage results.

Fig. 13 shows the estimated accumulative damage results. It can be seen from Fig. 10(a) that the accumulative damage of IGBT is 0.0915 (from 10 months of accumulation), and its corresponding lifetime is about 9.1 years. Similarly, the accumulative damage of diode is 0.0501 (From 10 months accumulation) in Fig. 10(b), and its corresponding lifetime is about 16.6 years. Please note that these parameters are inverter specific, so for PV inverters from different vendors the parameters are related to the semiconductor specs, PV inverter topology and rating. The team currently does not have all the specs for the PV inverters in the Mount Holly system, so the results are representative and will be refined once we know more about the detailed design and specifications from the inverter vendor.

According to the ten-month lifetime of the power device calculated as above, it can be obtained that the lifetime of the corresponding power device is a certain fixed value. This is often far from reality because variations in device parameters (uncertainties) and experienced thermal stresses are not considered. In practice, due to these uncertainties, the lifetime of power devices may vary within a certain range. Therefore, lifetime predictions are often expressed in terms of statistical values rather than fixed values [9]. Finally, a statistical approach based on the Monte Carlo analysis is applied, as shown in Fig. 14.

In this case, the parameters of the lifetime model in (5) are modeled using a normal distribution with a parameter variation of 5%,which can be seen in Fig. 15. Likewise, parameter changes also require the introduction of stress parameters ($T_{jm}$, $\Delta T_j$, and $t_{on}$), which are inputs to the lifetime model. In this case, it is necessary to determine the equivalent static values of these dynamic parameters (which change dynamically during operation, i.e., the mission profile). Basically, the equivalent static values of the stress parameters ($T'_{jm}$, $\Delta T'_j$ and $t'_{on}$) are representative of the stresses obtained from the mission profile, which results in the same lifetime. In fact, there are many combinations of equivalent static values that can be applied to the lifetime model and produce the same lifetime. For simplicity, only the line frequency (i.e. 50 Hz) thermal cycle is considered, that is, $t'_{on}$ is selected as 0.01 s (the heating period is half of the total cycle period), and the number of cycles per ten month $n'_i$ is (10×30×24×60×60 )×50 cycles. Regarding the junction temperature variation, the equivalent average junction temperature $T'_{jm}$ can be obtained by averaging the per ten month mission profile of the mean junction temperature [10]. Then, the equivalent cycle amplitude $\Delta T'j$ can be calculated by solving equation (5). Table V summarizes the equivalent static values from the mission profile. Once the equivalent static values are determined, they can also be modeled using a normal distribution function, as was done previously for the lifetime model parameters as shown in Fig. 16 and Fig. 17.

TABLE V EQUIVALENT STATIC VALUES OF THE STRESS PARAMETERS.

| | |
|---|---|
| Mean junction temperature $T'_{jm(IGBT/Diode)}$ | 24.9℃/24.2℃ |
| Cycle amplitude $\Delta T'_{j(IGBT/Diode)}$ | 0.12179℃/0.13954℃ |
| Cycle period $t'_{on}$ | 0.01s |
| Number of cycles per ten month $n'_i$ | (10×30×24×60×60 )×50 |
| Accumulative damage $AD_{(IGBT/Diode)}$ | 0.0915/0.0501 |
| Lifetime prediction $LP_{(IGBT/Diode)}$ | 9.1 years /16.6 years |

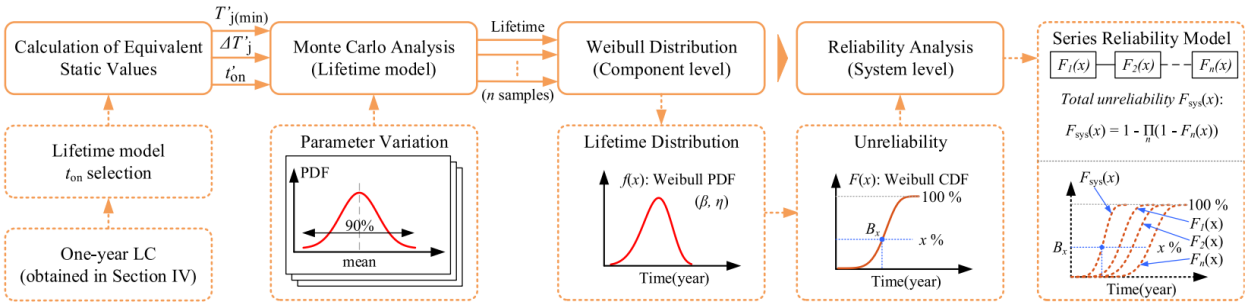


Fig. 14 Flow diagram of the reliability assessment of PV inverters with the Monte Carlo analysis and reliability block diagram. LC: lifetime consumption, $t_{on}$: heating time, $T'_j$(min): equivalent minimum junction temperature, $\Delta T'_j$ : equivalent cycle amplitude, $t'$on: equivalent heating time, $f(x)$: Weibull Probability density function (PDF), $\beta$: sharp parameter, $\eta$: scale parameter, $F(x)$: cumulative density function (CDF), $F_i(x)$: unreliability function of the $i$th device in the system, $F_{sys}(x)$: total unreliability of the system, and $B_x$ : operation time when $x$% of the populations fail [9].

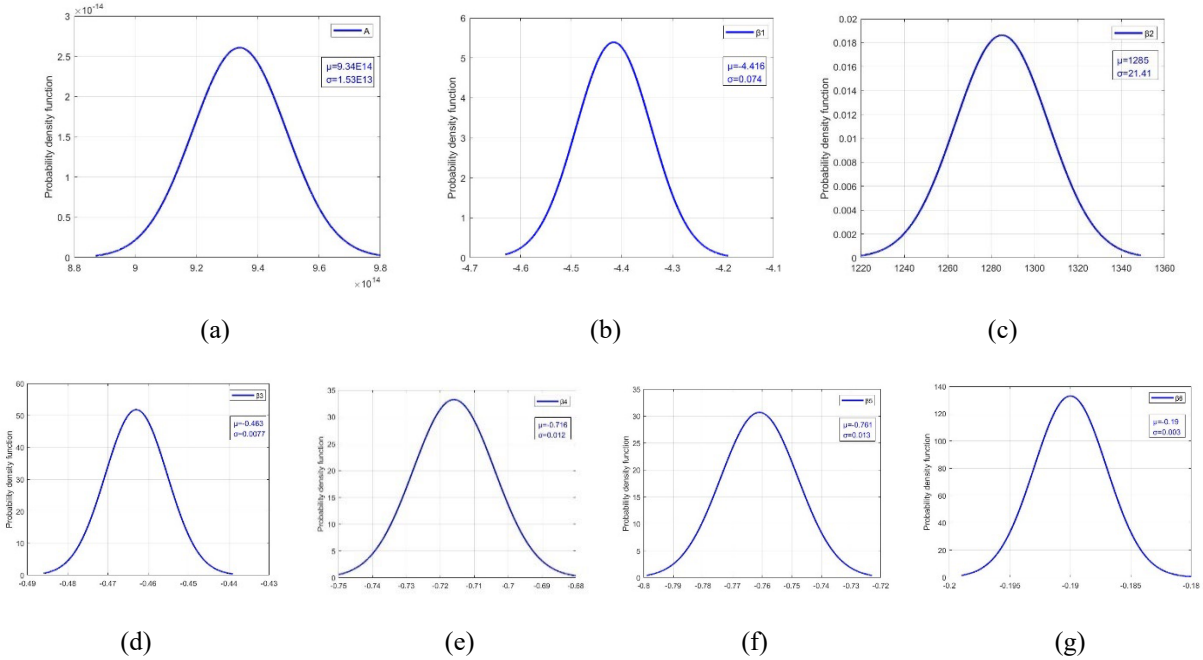


(a) (b) (c)

(d) (e) (f) (g)

Fig. 15. Normal distrbution of all lifetime model parameters(IGBT/Diode).

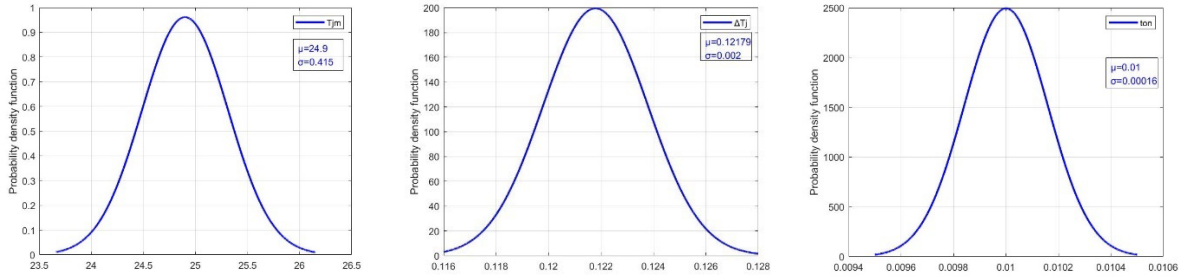


(a) (b) (c)

Fig. 16. Normal distrbution of all stress parameters (IGBT).

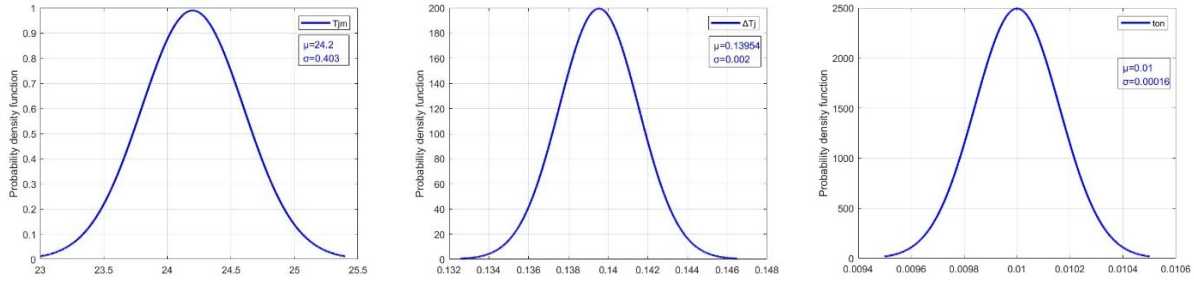


(a) (b) (c)

Fig. 17. Normal distrbution of all stress parameters (Diode).

In order to evaluate the impact of parameter variations on the annual damage of power semiconductor devices, a sensitivity analysis was performed by considering each individual

parameter variation while other parameters maintained the mean value of their distribution [11]. Each distribution is sampled using Monte Carlo simulation, with the number of samples determining the accuracy of the output distribution. Therefore, 10,000 samples were selected to establish the annual damage distribution. Considering seven parameters variations of the lifetime model, the annual damage distribution of the power semiconductor is shown in Fig. 18 and Fig. 19.

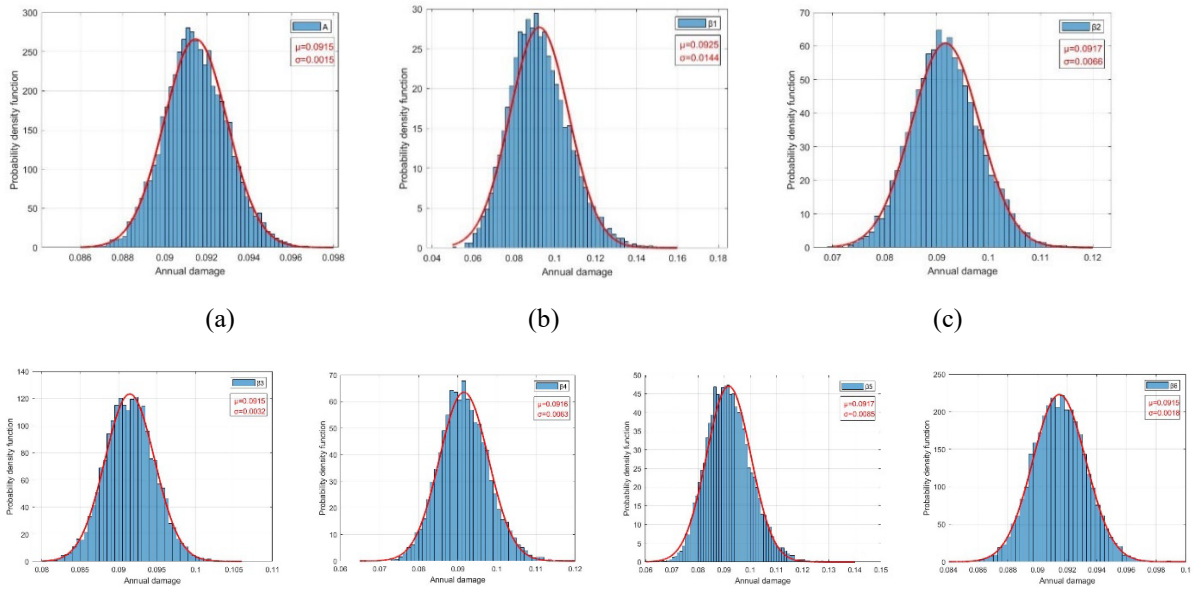


(a) (b) (c)

(d) (e) (f) (g)

Fig. 18. Annual damage distribution considering the individual parameter variation in the lifetime model (IGBT).

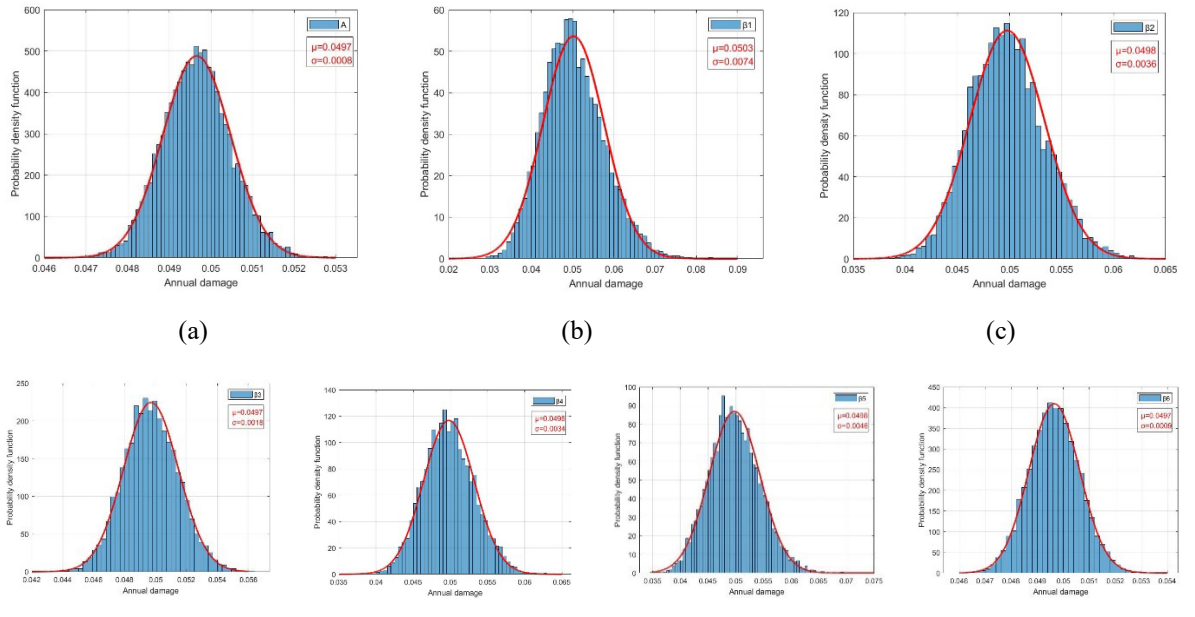


(a) (b) (c)

(d) (e) (f) (g)

Fig. 19. Annual damage distribution considering the individual parameter variation in the lifetime model (Diode).

As shown in the figure above, the blue bars represent the frequency of occurrence, while the red curve is the fitted pdf of the normal distribution. It is worth noting that when the $\beta_1$ is an exponential factor of junction temperature fluctuation, the annual damage deviation is the largest for IGBT, which indicates that the lifetime model is most sensitive to this factor. While the annual damage of these variations for Diode is almost consistent with the static value. Likewise, by using Monte Carlo simulation, a sensitivity analysis of the stress assessment can be calculated, as shown in Fig. 20 and Fig. 21. It is worth noting that the annual average damage of these variations is almost consistent with the static value.

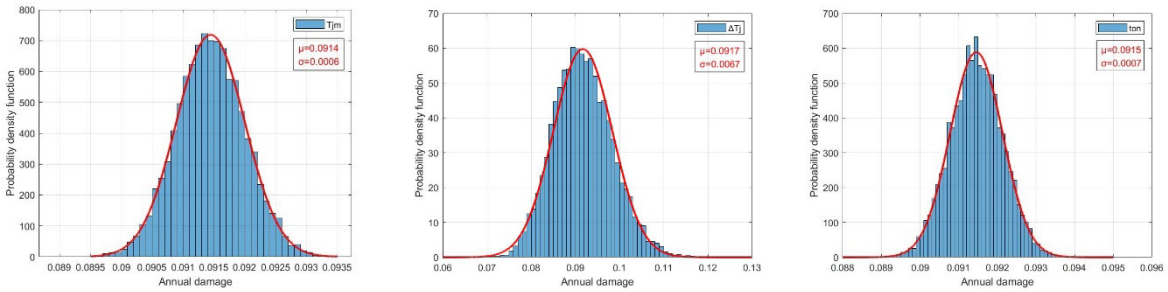


(a) (b) (c)

Fig. 20. Annual damage distribution considering individual parameter variation in stress (IGBT).

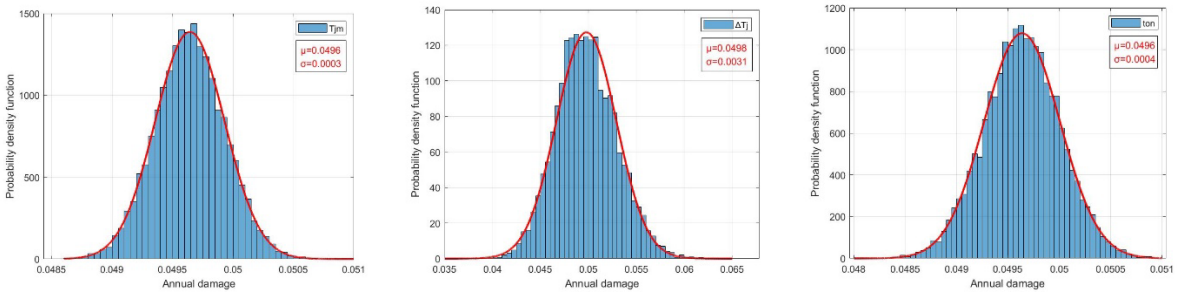


(a) (b) (c)

Fig. 21. Annual damage distribution considering individual parameter variation in stress (Diode).

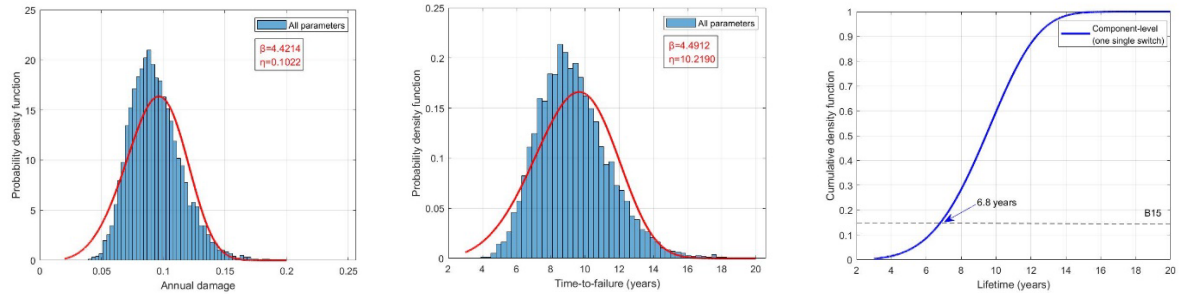


(a) (b) (c)

Fig. 22. Monte Carlo analysis considering all parameters variations from the stress evaluation and lifetime model. (a) Annual damage; (b) Time-to-failure distribution; (c) Cumulative density function (i.e. unreliability) along with the lifetime (IGBT).

Taking into account all parameter variations, using Monte Carlo simulation, the annual damage distribution is shown in Fig. 22(a) and Fig. 23(a) .

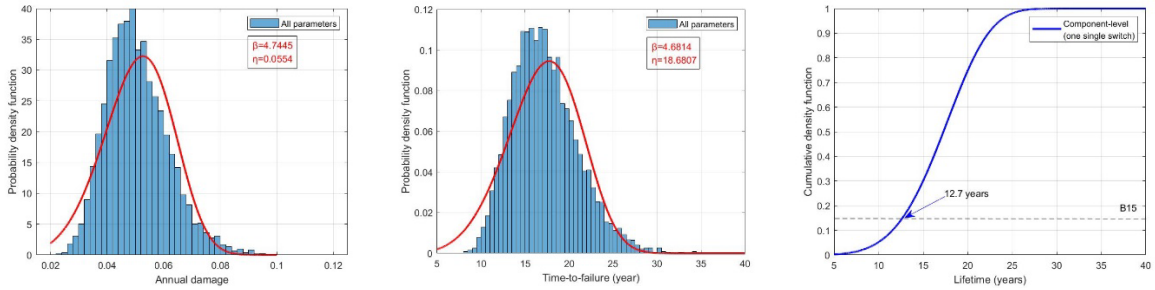


(a) (b) (c)

Fig. 23. Monte Carlo analysis considering all parameters variations from the stress evaluation and lifetime model. (a) Annual damage; (b) Time-to-failure distribution; (c) Cumulative density function (i.e. unreliability) along with the lifetime. (Diode).

It is known that time-to-failure usually follows the Weibull distribution[12],[13],whose PDF can be expressed as

$$f(x) = \frac{\beta}{\eta^{\beta}} x^{\beta-1} \exp\left[-\left(\frac{x}{\eta}\right)^{\beta}\right] \tag{6}$$

where $\beta$ is the shape parameter and $\eta$ is the scale parameter. Generally speaking, the value of $\beta$ represents a failure mode (i.e. the same failure mode will lead to similar $\beta$ value), while the value of $\eta$ is corresponding to the time when 63.2% of population will have failed [12].The fitting curve can be obtained with the corresponding scale paremeter and shape paremeter. Assuming that the mission profile is repeated every year, the lifetime probability distribution is shown in Fig. 22(b) and Fig. 23(b) . In fact, it can be seen that the scale parameter of IGBT is 10.2190 which is lower compared to Diode, although the average lifetime of Diode is higher than IGBT. Thus, the cumulative density functions of the lifetime are derived by integrating the corresponding PDF from -∞ to t, with the results being shown in Fig. 22(c) and Fig. 23(c). Typically, reliability is expressed in terms of B15 lifetime, which is the time required for 15% of the population to fail [14]. Therefore, by considering the unreliability function, the reliability or B15 lifetime of the semiconductor switch can be obtained. Obviously, the B15 lifetime of a single IGBT and Diode in the converter represents a reliability of 6.8 years and 12.7 years respectively.

## III. System-Level Reliability Analysis

According to the component-level unreliability function $F(x)$ obtained by the Monte Carlo method, the system-level reliability assessment can be carried out using the reliability block diagram [15], as shown in Fig. 24. The three-phase two-level inverter topology in Figure 11 consists of six power devices. If any one device fails, the inverter will not work. Therefore, the total unreliability of the system $F_{sys}(x)$ can be calculated as

$$F_{\text{sys}}(x) = 1 - \prod_{n=1}^{6}\left(1 - F_n(\text{x})\right) \tag{7}$$

where $F_{\text{n}}(x)$ is the unreliability function of the n$^{\text{th}}$ power device in the system. In the case of three-phase two-level inverter topology (with bipolar pulse width modulation technique), the loading of each power device is equal [10], which means it has the same unreliability function: $F(x) = F_1(x) = F_2(x) = F_3(x) = F_4(x) = F_5(x) = F_6(x)$.Therefore, the system-level unreliability function can be simplified as

$$F_{\text{sys}}(x) = 1 - (1 - F(x))^6 \tag{8}$$

The system-level unreliability functions of the converters are presented in Fig. 25, together with the corresponding system-level B15 lifetimes. The system-level B15 lifetime or the reliability of the IGBT is 4.6 years, which is 2.2 years lower than the component-level B15 lifetime. Moreover, the system-level B15 lifetime or the reliability of the Diode is 8.6 years, which is 4.1 years lower than the component-level B15 lifetime. It's worthy mentioning that the system-level unreliability is always higher than the component-level unreliability, because the main reason is that the more devices you have, the more chances of failure.

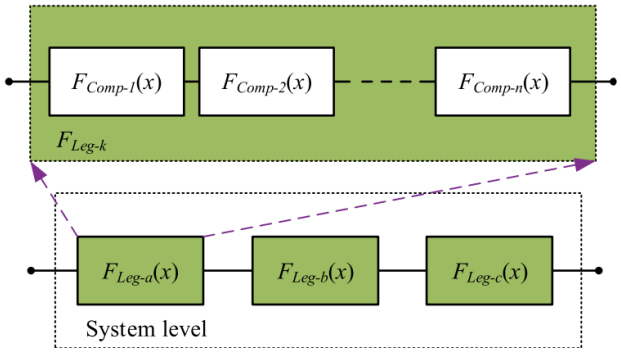


Fig. 24. Series connection of reliability block diagram of a three-phase two-level inverter, where $F_{\text{Comp-i}}(x)$ represents the unreliability function of the ith device in the inverter leg and the subscript Leg-k denotes the *a*, *b*, or *c* phase [9].

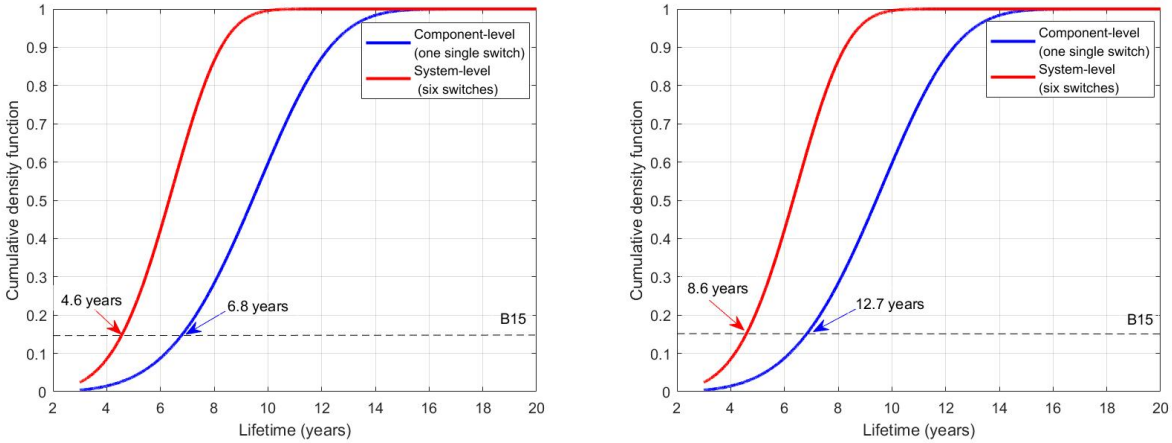


(a) (b)

Fig. 25. Component-level and system-level unreliability functions of the converter.(a) IGBT. (b) Diode.

In summary, the framework of the proposed reliability assessment tool for PV inverters by utilizing the PV system reliability-related information (such as energy mission profile, semiconductor temperature and stress, temperature, etc.) to quantify and compare the reliabilities for PV inverter from different vendors with different control methods. The lifetime prediction for the PV inverter leads to a better understanding of the number of thermal cycles to failure. And the remaining lifetime of main components (IGBT, Diode, MOSFET, etc.,) can be estimated forewarningly. Based on this reliability assessment platform, predictive maintenance and reliability-oriented control and operation methods, such as active thermal control, can be implemented to extend the lifetime of PV inverters. This approach helps PV inverter designers select the most cost-effective power device and justify the corresponding risk of unreliability among the options available in the market for a specific PV inverter application. Additionally, by using system-level reliability assessment, the obtained lifetime results can be used in a comparative manner to evaluate the impact of the PV inverter topology on the expected lifetime of the PV inverter system.

## IV. REFERENCE

[1] Jordan D.C, Marion B., Deline C. Barnes T., Bolinger M., PV field reliability status—Analysis of 100 000 solar systems, Progress in PV 28 (8), 2020, 739 – 754.

[2] K. Ma, M. Liserre, F. Blaabjerg and T. Kerekes, "Thermal Loading and Lifetime Estimation for Power Device Considering Mission Profiles in Wind Power Converter," IEEE Trans. Power Electron., vol. 30, no. 2, pp. 590-602, Feb. 2015.

[3] U.-M. Choi, K. Ma, and F. Blaabjerg, "Validation of lifetime prediction of IGBT modules based on linear damage accumulation by means of superimposed power cycling tests," IEEE Trans. Ind. Electron., vol. 65, no. 4, pp. 3520–3529, Apr. 2018.

[4] L. Wang, J. He, T. Han, and T. Zhao, "Finite control set model predictive control with secondary problem formulation for power loss and thermal stress reductions," IEEE Trans. Ind. Appl., vol. 56, no. 04, pp. 4028–4039, Jul./Aug. 2020.

[5] A. Ammous, S. Ghedira, B. Allard, H. Morel, and D. Renault, "Choosing a thermal model for electrothermal simulation of power semiconductor devices," IEEE Trans. Power Electron., vol. 14, no. 2, pp. 300–307, Mar. 1999.

[6] R. Bayerer, T. Herrmann, T. Licht, J. Lutz, and M. Feller, “Model for power cycling lifetime of igbt modules - various factors influencing lifetime,” in 5th International Conference on Integrated Power Electronics Systems, 2008, pp. 1–6.

[7] L. Wang, T. Zhao, and J. He, "Investigation of Variable Switching Frequency in Finite Control Set Model Predictive Control on Grid-Connected Inverters", in IEEE Open Journal of Industry Application, 2021.

[8] L. Wang, T. Zhao and J. He, "Centralized Thermal Stress Oriented Dispatch Strategy for Paralleled Grid-Connected Inverters Considering Mission Profiles," in IEEE Open Journal of Power Electronics, 2021.

[9] J. He, A. Sangwongwanich, Y. Yang, and F. Iannuzzo, "Lifetime Evaluation of Three-Level Inverters for 1500-V Photovoltaic Systems," IEEE J. Emerg. Sel. Topics Power Electron., vol. 9, no. 4, pp. 4285-4298, Aug. 2021.

[10] Y. Yang, A. Sangwongwanich, and F. Blaabjerg, “Design for reliabilityof power electronics for grid-connected photovoltaic systems,” CPSS Trans. Power Electron. Appl., vol. 1, no. 1, pp. 92–103, Dec. 2016.

[11] D. Zhou, H. Wang, F.Blaabjerg,S. K. Kaer, and D. Blom-Hansen, “System-level reliability assessment of power Stage in fuel cell application,” in Proc. ECCE,Sept.2016,pp.1-8.

[12]H.S.-H.Chung, H. Wang, F.Blaabjerg, and M.Pecht, Reliability of Power Electronic Converter Systems. *IET*,2015.

[13] ZVEI, “How to measure lifetime for Robustness Validation – step by step,”*Rev*.1.9,Nov.2012.

[14]M. Sandelic, A. Sangwongwanich and F. Blaabjerg, “Reliability evaluation of PV systems with integrated battery energy storage systems: DC-coupled and AC-coupled configurations,” Electron., no.8, pp. 1059, 2019.

[15] D. Smith, Reliability, Maintainability and Risk: Practical Methods for Engineers. Amsterdam, The Netherlands:Elsevier, 2017. [Online]. Available: https://books.google.dk/books?id=zLgxDQAAQBAJ